Route-and-Execute: Auditable Model-Card Matching and Specialty-Level Deployment

Shayan Vassef SHAYAN@NIMBLEMIND.AI
Nimblemind, USA

Soorya Ram Shimgekar SOORYA@NIMBLEMIND.AI
Nimblemind, USA

Abhay Goyal ABHAY@NIMBLEMIND.AI
Nimblemind, USA

Koustuv Saha KSAHA2@ILLINOIS.EDU
University of Illinois - Urbana Champaign, IL, USA

Pi Zonooz PI@NIMBLEMIND.AI
Nimblemind.ai, USA

Navin Kumar NAVIN@NIMBLEMIND.AI
Nimblemind.ai, USA

Abstract

Clinical workflows are fragmented as a patchwork of scripts and task-specific networks that often handle triage, task selection, and model deployment. These pipelines are rarely streamlined for data science pipeline, reducing efficiency and raising operational costs. Workflows also lack data-driven model identification (from imaging/tabular inputs) and standardized delivery of model outputs. In response, we present a practical, healthcare-first framework that uses a *single* vision–language model (VLM) in two complementary roles. **First (Solution 1),** the VLM acts as an aware model-card matcher that routes an incoming image to the appropriate specialist model via a three-stage workflow (modality → primary abnormality → model-card id). Checks are provided by (i) stagewise prompts that allow early exit via `None`/`Normal`/`Other` and (ii) a stagewise answer selector that arbitrates between the top-2 candidates at each stage, reducing the chance of an incorrect selection and aligning the workflow with clinical risk tolerance. **Second (Solution 2),** we fine-tune the VLM on specialty-specific datasets ensuring a single model covers multiple downstream tasks within each specialty, maintaining performance while simplifying deployment. Across gastroenterology, hematology, ophthalmology, and pathology, our single-model deployment matches or approaches specialized baselines.

Compared with pipelines composed of many task-specific agents, this approach shows that one VLM can both *decide* and *do*. It may reduce effort by data scientists, shorten monitoring, increase the transparency of model selection (with per-stage justifications), and lower integration overhead.

Keywords: Healthcare AI, Vision–Language Models, MedGemma, Model Cards, MLOps, Early termination, Confidence thresholds, Selective prediction

Data and Code Availability Data and code are available from the authors at reasonable request.

Institutional Review Board (IRB) All data is publicly available and de-identified; the study is IRB-exempt.

1. Introduction

Machine learning (ML) models in healthcare face significant operational friction when moving from research prototypes to clinical practice. An estimated 90% of medical AI models never reach clinical deployment Poddar et al. (2024), and production-ready models can take weeks to months to integrate, with over half of organizations reporting 8–90 days to deploy a single model Mage AI (2025). These delays

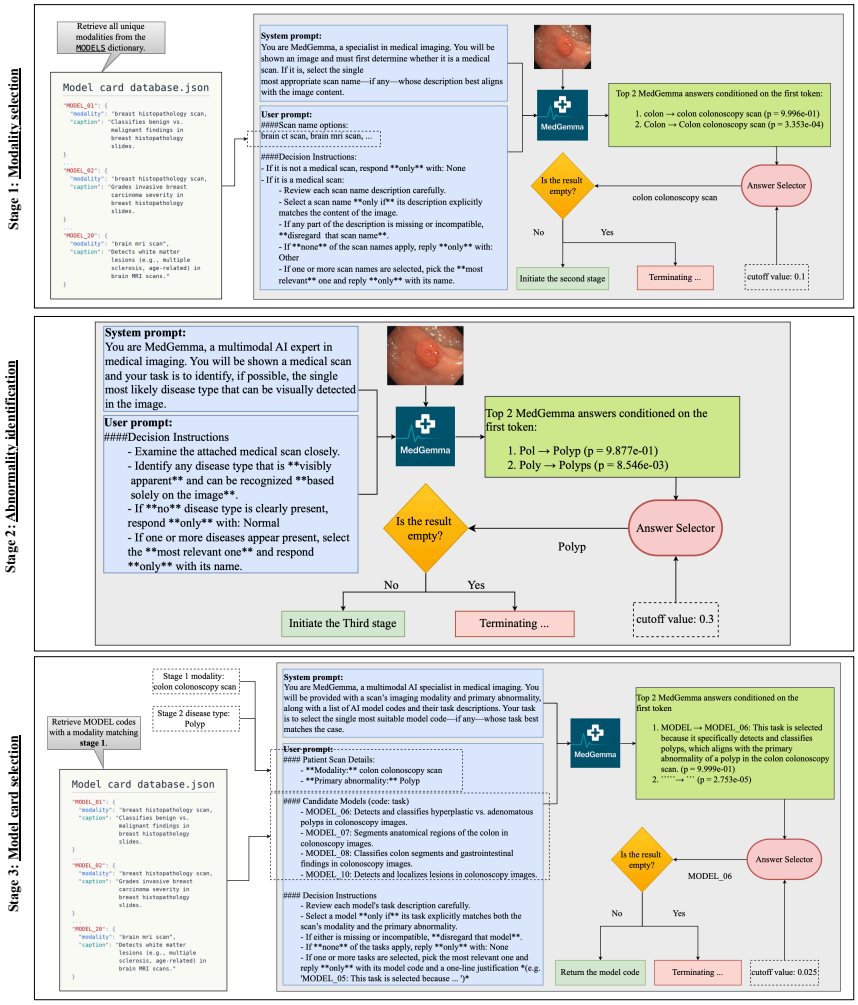

Figure 1: Three-stage model-card matching workflow (modality → abnormality → model card id).

stem from several bottlenecks, and we provide two key examples here. First, to select an appropriate model design (architecture, training objective, etc.) for a given dataset, the data scientist must identify the attributes that should guide the design. In tabular data these attributes are explicit; in clinical images they are latent in the pixels—such as *modality* (e.g., CT) and *clinical indication* (e.g., acute intracranial hemorrhage)—and must first be extracted, standardized, and quality-checked before they can inform design choices. As a result, streamlined model selection for clinical imaging is often overlooked and warrants dedicated attention (Willemink et al., 2020). Second, each chosen model is an operational artifact: health systems integrate, validate, monitor, and recalibrate AI solutions one by one, so developing and maintaining task-specific models multiplies the cost burden and slows adoption (Brady et al., 2024).

We address these operational issues with two linked solutions: the first assists data scientists in selecting the appropriate model, and the second outlines a practical first step to shorten time-to-deployment once that selection is finalized.

Solution 1: Model-card matching Early medical vision–language efforts aligned images and text to enable cross-modal understanding and transfer. Recently, MedGemma Sellergren et al. (2025) and UMIT Yu et al. (2025) showed that medical VLMs can approach specialized systems while maintaining generality, motivating workflows that both interpret

the input and decide what to do next. As such, we adopt a medical VLM as an aware, auditable selector that reads an input image and chooses an appropriate model card via a three-stage pipeline (MODALITY → PRIMARY ABNORMALITY → MODEL-CARD ID). At each stage, the VLM proposes top candidate models, and an answer selector applies a calibrated threshold that can abstain and, when appropriate, terminate early to prevent error cascades. Decisions at each stage (VLM output, any abstention, and routing to the next stage) are visible to users and logged in a consistent format, yielding transparent selection tied to model-card semantics (Mitchell et al., 2019) and safe selective prediction (Geifman and El-Yaniv, 2019). This process accelerates development: We believe that choosing the appropriate model for a given clinical image hinges on two key pieces of information—imaging modality and disease type—details that are not always apparent to data scientists.

Solution 2: Specialty-specific deployment Prior work shows that domain-pretrained medical encoders, when fine-tuned on target tasks, can match strong baselines across multiple datasets (Zhang et al., 2022; Mei et al., 2022). In healthcare, specialty-level foundation models have also demonstrated broad coverage within a specialty—outperforming narrow, dataset-specific models across many tasks (e.g., pathology's Prov-GigaPath achieves SOTA on 25/26 tasks across 31 tissue types) (Xu et al., 2024). Operationally, fewer, broader specialty models reduce the number of artifacts a health system must validate, secure, and monitor, lowering deployment burden compared with one-model-per-dataset estates (Brady et al., 2024). In line with past work, we fine-tune the same calibrated VLM at the *specialty* level—gastroenterology, hematology, ophthalmology, and pathology—rather than per dataset. Our goal is to match task-specific model performance while keeping everything on a single, easy-to-maintain deployment stack. Once a model card is finalized by the joint decision of the data scientist and the Solution 1 selection workflow, the data scientist can adapt the VLM to the downstream use case rather than designing a new model. This adaptation consists of tailoring the VLM prompt to the use case and eliminates the time otherwise spent building and integrating a new architecture.

Taken together, these solutions link selection and deployment in a single, calibrated workflow—a VLM that can *route and execute*. Compared with recent multi-agent pipelines (Shimgekar et al., 2025), this minimalist design may reduce data-science workload and reduce human error. As an example, AI-driven triage has been shown to cut chest-radiograph reporting delays from 11.2 to 2.7 days in simulation while maintaining diagnostic performance (Annarumma et al., 2019). Similarly, our approach may shorten the path from triage to clinical use and increase throughput without sacrificing performance.

2. Related Work

Automated matching in healthcare Matching models based on an appropriate dataset has been explored at multiple layers of care delivery, such as patient-facing systems, specialty care, etc. Patient-facing systems (e.g., symptom checkers like Buoy Health buoy health (2025)) narrow likely conditions and suggest next steps. Platforms such as Garner Health Garner (2025) match patients to specialists using outcomes data. Similarly, LLM-driven controllers (HuggingGPT Shen et al. (2023)) show how a coordinator can parse requests, consult model descriptions, and delegate to expert models. This pattern maps naturally to healthcare *model cards* as standardized summaries of intended use and performance Mitchell et al. (2019). Clinical imaging "orchestration" seeks to run the appropriate algorithm on the selected scan Aidoc (2024). However, prior work does not provide calibrated, stage-wise routing that is explicitly grounded in model-card semantics, with visible abstention and early termination and per-stage decision logs for audit. In the first solution, we address this gap with a three-stage router that makes every decision—VLM output, abstention, and route—user-visible and logged, cutting routing errors while preserving safety via careful prompt design and stage-specific selection logic.

Adaptation across tasks A parallel line of work reduces packaging and integration friction for *multiple* models: MONAI Project MONAI (2023) deploys standardized applications, packaging and interfaces, and self-configuring pipelines like nnU-Net Isensee et al. (2021) that adapt architectures to new datasets with minimal manual tuning. In practice, however, maintaining one network per task is inefficient: each model has to be validated, integrated, monitored, and updated separately at the site level, duplicating effort and slowing adoption (Brady et al., 2024; Boverhof et al., 2024). Multi-agent or model-zoo deployments

likewise increase the number of components to secure, monitor, and recalibrate over time, compounding technical debt (Sculley et al., 2015). Unlike UMIT Yu et al. (2025)—which initializes Qwen2-VL Wang et al. (2024) and follows a two-stage pipeline (full-parameter feature alignment followed by instruction fine-tuning) to reach competitive results across many datasets and modalities—there is no evidence that a single calibrated VLM can be *reused* across specialties within one unified deployment stack where onboarding a new task changes only the *user prompt*. Our second solution targets this gap: we fine-tune one medical VLM across datasets within a specialty so a single component serves multiple imaging tasks, keeping interfaces and calibration fixed while matching or approaching benchmark performance.

3. Solution 1: Model–Card Matching with Early Termination

To integrate the medical VLM as an automated model selector, we use a three-stage prompting pipeline. At each stage, the model receives a specific instruction and context to return a textual answer. The stages progressively narrow the information needed to select the appropriate model card. After each response, an **answer selection** step ranks all candidate answers by likelihood, retains the top two, and then decides whether to proceed to the next stage or terminate early. Figure 1 illustrates the overall workflow, and Algorithm 1 gives pseudocode for the answer-selection strategy. Below, we first outline the prerequisites and then describe the selection process for each stage.

Prerequisite 1: Backbone VLM choice In Section 1 (Solution 1) we described a generic medical VLM; here, we *adopt* MedGemma. MedGemma was pretrained on a multi-modal medical mixture spanning radiology (CXR/CT/MRI), ophthalmology, dermatology, and histopathology[1] and reports competitive benchmarks relative to prior work Sellergren et al. (2025).

Prerequisite 2: Model-card repository To match a clinical image to the correct model, we maintain a diverse repository of model cards spanning multiple modalities (e.g., CT, MRI) and AI tasks (e.g., classification, grading). Instead of storing task-specific models, each candidate is indexed by a string key—the *model-card ID* (a.k.a. model code; e.g., `MODEL_04`, which might refer to an ophthalmology model)—and two minimal descriptors that make it discoverable by the router: (i) a short *task caption* describing what the model does (e.g., "segments tumor regions in histopathology images"), and (ii) the *modality*, i.e., the scan type on which the model was trained (e.g., "breast histopathology scan").

Stage 1: Modality identification The goal of the first stage is to determine the imaging modality or scan type of the input image. We prompt MedGemma with a system message that casts it as a medical-imaging specialist and supply a list of admissible modalities drawn from the model-card repository. Concretely, we iterate over all model cards, extract each card's `modality` field, deduplicate the values to form a unique set, and inject that set into the prompt. The prompt instructs: (1) if the image is *not* a medical scan, respond with "None"; (2) if it is a medical scan, choose the single most appropriate scan name from the list that matches the image content; and (3) if none of the listed modalities perfectly fits, respond with "Other." This prompting strategy explicitly conditions the model to use the tokens "None" or "Other" as outputs in the absence of a confident match. For example, given an endoscopic image, the correct output might be "Colonoscopy"; for a non-medical photograph (e.g. a picture of a cat), the model should output "None."

Stage 2: Primary finding detection In the second stage, the model examines the image (knowing the modality from Stage 1) and attempts to identify the primary abnormality or finding, if any. We prompt MedGemma with an instruction such as: "Identify the single most likely disease or finding apparent in this scan. If no disease is present, respond only with: 'Normal.'" This stage is essentially an image-based diagnosis step for a high- level finding. For example, given a colonoscopy image, the model might answer "Polyp" if one is seen; given a chest X-ray, it might answer "Normal" if nothing abnormal stands out, or a broad condition like "Pneumonia" if detected. The prompting ensures that the special token "Normal" is used to indicate the absence of any visible pathology.

Stage 3: Model-card selection In the final stage, the model selects an appropriate card from

1. Example datasets: MIMIC-CXR 231,483 images; EyePACS 199,258; internal dermatology 51,049; PAD-UFES-20 2,047; internal histopathology 32.55M patches; CT-US1 59,979 slices; MRI-US1 47,622 (Sellergren et al., 2025).

Table 1: Performance summary across specialties

Task	External benchmark	MedGemma	(S–S) fine-tuned	(M–S) fine-tuned
Gastroenterology — *PolypSet* (Train: 27,048; Test: 4,719; Val: 4,214)				
Polyp Classification (Acc.)	81%	61%	79%	—
Polyp Classification (F1 Macro)	80%	38%	77%	—
Polyp Classification (F1 Weighted)	81%	47%	79%	—
BBox Localization Acc.	78%	1%	—	—
Region Localization Acc.	—	32%	46%	—
Hematology — *BloodMNIST* (Train: 11,959; Test: 3,421; Val: 1,712)				
Cell-type Classification (Acc.)	97%	20%	98%	—
Cell-type Classification (F1 Macro)	—	8%	98%	—
Cell-type Classification (F1 Weighted)	—	10%	98%	—
Ophthalmology — *OCTMNIST* (Train: 97,477; Test: 1,000; Val: 10,832)				
Retinal OCT Classification (Acc.)	78%	26%	93%	—
Retinal OCT Classification (F1 Macro)	—	38%	77%	—
Retinal OCT Classification (F1 Weighted)	—	47%	79%	—
Ophthalmology — *RetinaMNIST* (Train: 1,080; Test: 400; Val: 120)				
Diabetic Retinopathy Grading (Acc.)	53%	55%	74%	—
Diabetic Retinopathy Grading (F1 Macro)	—	37%	59%	—
Diabetic Retinopathy Grading (F1 Weighted)	—	52%	72%	—
Pathology — *TissueMNIST* (Train: 165,466; Test: 47,280; Val: 23,640)				
Kidney Cortex Classification (Acc.)	70.3%	21%	70.1%	28%
Kidney Cortex Classification (F1 Macro)	—	5%	60%	—
Kidney Cortex Classification (F1 Weighted)	—	9%	69%	—
Pathology — *PathMNIST* (Train: 89,996; Test: 7,180; Val: 10,004)				
Tissue Type Classification (Acc.)	91.1%	38%	96%	21%
Tissue Type Classification (F1 Macro)	—	28%	94%	—
Tissue Type Classification (F1 Weighted)	—	29%	96%	—
Pathology — *BreastHIST* (Train: 214,969; Test: 31,376; Val: 31,179)				
Ductal Carcinoma Classification (Acc.)	84.3%	69%	87%	32%
Ductal Carcinoma Classification (F1 Macro)	—	66%	84%	—
Ductal Carcinoma Classification (F1 Weighted)	—	70%	87%	—

the repository. We iterate over all cards, filter to those whose `modality` matches the Stage 1 choice, and pass the resulting list of `(model_card_id, task_caption)` pairs to the prompt. For example, if Stage 1 predicts `breast histopathology scan`, the candidate set might be: [`MODEL_01: Classifies benign vs. malignant findings in breast histopathology slides.`, `MODEL_04: ...`]

To give the model sufficient context to decide among these candidates, we include the Stage 1 modality and the Stage 2 primary abnormality as structured fields in the prompt (e.g., *Patient scan details*: breast histopathology scan; *Primary abnormality*: carcinoma). To make this a pure selection task, we mask the input image so that MedGemma acts as a language model solving a multiple-choice problem over the candidate list. The prompt instructs the model to: (i) review each candidate's task caption; (ii) select a model only if its task explicitly matches *both* the identified modality and abnormality; (iii) reply `None` if no option fits; and (iv) when a match exists, return the model's code (card ID) plus a one-line justification of the fit.

Answer selector and arbitration Despite careful prompt engineering at each stage—using cues like `return the best-matched`, emphasizing control words (e.g., `only`), and explicitly listing abstention options (e.g., `None`)—the workflow still underweights abstentions (`None`, `Other`, `Normal`). This can compromise safety by increasing false selections when abstention would be preferable. Token-level analysis of secondary candidates shows that abstention terms frequently appear as the second-most likely answers. Accordingly, we shift from committing to the single top candidate to also considering the second-ranked candidate. We detail this change in the following:

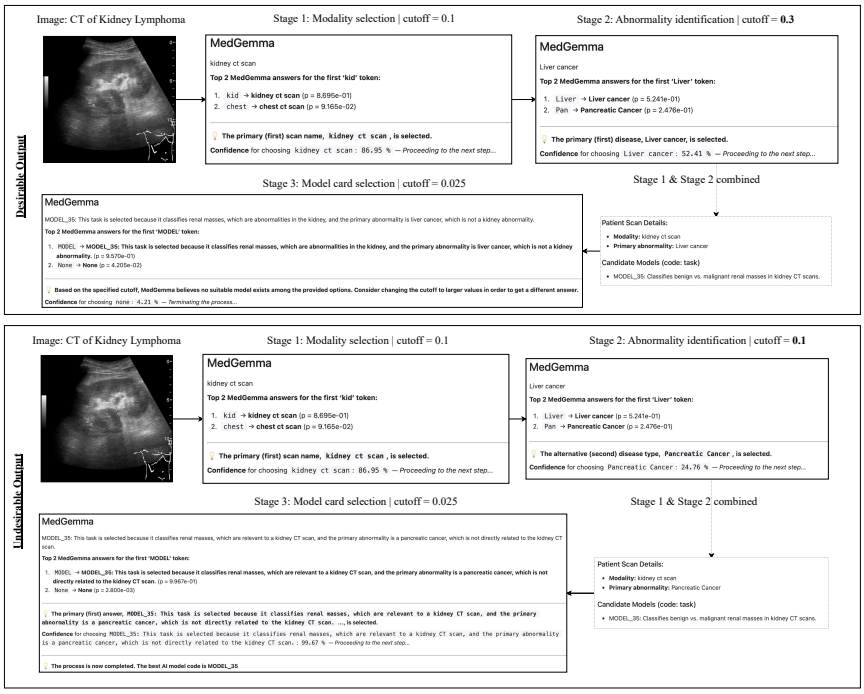

Figure 2: Effect of Stage 2 and Stage 3 cutoffs on the *same* renal ultrasound image. **Top:** higher τ_2=0.30 with small τ_3=0.025 triggers early termination (`None`). **Bottom:** lower τ_2=0.10 with the same τ_3=0.025 fails to halt, yielding an incorrect model-card id.

Algorithm 1: Answer selector (per stage)

Input: Candidate list $\mathcal{C} = \{(a_i, p_i)\}_{i=1}^{|V|}$ with $p_1 \geq p_2 \geq \cdots$; cutoff τ; abstain set $\mathcal{A} = \{\texttt{None}, \texttt{Normal}, \texttt{Other}\}$.
Output: Tuple $(y, \textsf{TERMINATE})$ or $(y, \textsf{PROCEED})$.

$(a_1, p_1), (a_2, p_2) \leftarrow$ top-2 from $\mathcal{C}$; $y \leftarrow a_1$
if $p_2 \geq \tau$ ***and*** $a_2 \neq a_1$ **then**
  $y \leftarrow a_2$ ▷ `prefer runner-up if sufficiently likely`
if $y \in \mathcal{A}$ **then**
  return $(y, \textsf{TERMINATE})$
return $(y, \textsf{PROCEED})$

Selector logic At each stage, we compute the distribution over the *first token*, sort the vocabulary by probability, and obtain a ranked list $\{(t_i, p_i)\}_{i=1}^{|\mathcal{V}|}$, where t_i is the i-th ranked first token and p_i is its probability. We then take the top two $\{(t_i, p_i)\}_{i=1}^{2}$ and decode full answers conditioned on each first token, yielding $\{(a_i, p_i)\}_{i=1}^{2}$, where a_i is the complete answer produced when the first token is fixed to t_i. This pair of candidates is passed to a transparent *answer selector* that arbitrates between the two using a stage-specific cutoff τ. This gives meaningful probability mass to abstentions (`None`/`Normal`/`Other`), which are often the runner-up.

Cutoffs in practice The purpose of per-stage cutoffs is to steer the workflow toward a more accurate outcome: either terminate early when plausible or return the best-matching model card (model code). Early termination can occur at any of the three stages—returning `None` or `Other` at Stage 1, `Normal` at Stage 2, or `None` at Stage 3—otherwise the pipeline outputs a model card id. To choose the cutoffs, we experimented on a broad set of out-of-distribution (OOD) clinical images, defined as any image outside MedGemma's training/validation/test sets, drawn from the datasets in Section 4 and from public, license-free images (Wikimedia Foundation, 2025). The resulting thresholds were a *low* cutoff at Stage 1 (0.10), a *moderate* cutoff at Stage 2 (0.30), and a *very small* cutoff at Stage 3 (0.025). **Figure 2** illustrates how the Stage 2 and Stage 3 thresholds can jointly flip the final outcome on the *same* renal ultrasound image (Hansen et al., 2015). In this example, Stage 2 is incorrect (the top-two predicted abnormalities are wrong). If Stage 2 forwards its

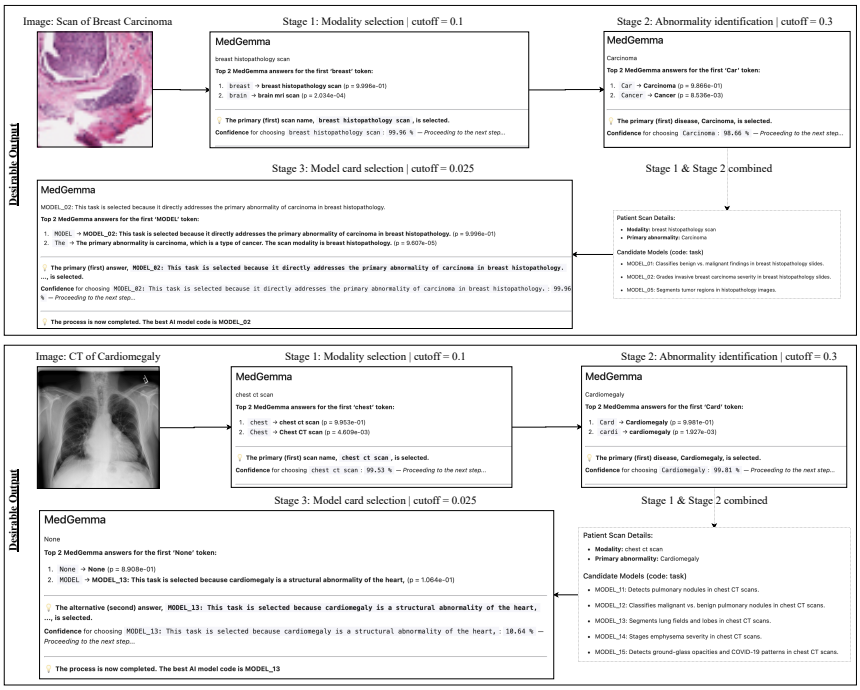

Figure 3: Two fixed-cutoff examples (τ_1=0.1, τ_2=0.3, τ_3=0.025) with correct final selections. **Top:** an easy case in which the thresholds have no effect. **Bottom:** a case where the very small Stage 3 cutoff allows the pipeline to select the correct model code.

first candidate to Stage 3 (bottom panel), an incorrect model card is selected given the cutoff threshold. By contrast, if Stage 2 instead forwards the second candidate (pancreatic cancer; top panel), the workflow abstains, returning `None`. Thus, the interplay between the Stage 2 candidate choice and the Stage 3 cutoff can flip the decision from a wrong selection to safe early termination. **Figure 3** illustrates two fixed–cutoff cases. *Bottom:* the very small Stage 3 cutoff allows the pipeline to select the second-ranked answer—a plausible model-card id for a chest X-ray with cardiomegaly from the NIH Long-Tail CXR dataset (Wang et al., 2017)—rather than terminate and return `None`. This example shows that the Stage 3 threshold was calibrated so that, when sufficiently likely, a second candidate can be prioritized over the first (abstention) option. *Top:* when the pipeline is highly confident at each stage—for a histopathology image with carcinoma from (Cruz-Roa et al., 2014)—the cutoffs are effectively inert and do not alter the outcome.

4. Solution 2: Specialty-specific model for downstream deployment

Building on the rationale in Section 1 (Solution 2), we fine-tune the same backbone VLM adopted in Section 3—MedGemma—across four specialties—gastroenterology, hematology, ophthalmology, and pathology—to simplify maintenance and deployment rather than pursue state-of-the-art performance on each task. For each specialty we compare: (a) an external task-specific benchmark (typically the published SOTA for that dataset), (b) the base MedGemma in zero-shot mode (no domain adaptation), and (c) MedGemma after specialty-specific fine-tuning (denoted "S–S" in the table). This tests whether a single specialty-tuned MedGemma can substitute for the external benchmark while keeping one deployment stack. If successful, a fixed VLM plus targeted prompt engineering and supervised fine-tuning may reduce the need to design, validate, and operate separate architectures—saving compute and shortening triage-to-deployment cycles Annarumma et al. (2019). We also evaluate multi-specialty fine-

tuning; details appear below under **Fine-tuning results**. All results are summarized in Table 1.

Datasets For gastroenterology, we use the dataset introduced by Li et al. (2021), an annotated compilation of three public sources: CVC-ColonDB Bernal et al. (2012), GLRC Mesejo et al. (2016), and KUMC (80 colonoscopy video sequences from the University of Kansas Medical Center). For hematology, we use BloodMNIST Acevedo et al. (2020), organized into eight blood cell categories. For ophthalmology, we employ OCTMNIST Kermany et al. (2018) (4 retinal OCT classes) and RetinaMNIST Dataset (2020) (5 retinopathy grades). For pathology, we use TissueMNIST Ljosa et al. (2012) (8 kidney cortex cell types), PathMNIST Kather et al. (2019) (9 colorectal tissue types), and a breast cancer histopathology set following Cruz-Roa et al. (2014). Train/validation/test sizes are summarized in Table 1.

Fine-tuning results We evaluate two approaches: *single-specialty* fine-tuning (training on all datasets within one specialty) and *multi-specialty* fine-tuning (training across multiple specialties). For both approaches, we use the same parameter-efficient fine-tuning (PEFT) method, QLoRA (Dettmers et al., 2023). As shown in Table 1, single-specialty fine-tuning substantially narrows the gap to specialist benchmarks. While the base MedGemma performs modestly in zero-shot mode, targeted specialty adaptation yields competitive results across modalities and objectives. This supports the premise that one VLM can act as a generalist engine per specialty, reducing the need for separate per-task architectures and thereby saving compute and shortening triage-to-deployment cycles.

For multi-specialty fine-tuning (column "M–S fine-tuned"), we perform *sequential* adaptation from a pathology-tuned model to ophthalmology. Operationally, this may be preferable to single-specialty models because a single multi-specialty model can serve more inputs routed by Solution 1, reducing the number of deployed variants. As a supplementary experiment, we assess retention by measuring performance on the pathology datasets (three rows in the table). The results show that sequentially fine-tuning from pathology to ophthalmology degrades performance on pathology—an instance of catastrophic forgetting Kirkpatrick et al. (2017). This suggests that, in healthcare settings, specialty-specific models may be a better default than multi-specialty models obtained via plain sequential fine-tuning; more advanced strategies such as multi-task (joint) fine-tuning Caruana (1997) or replay buffers Rebuffi et al. (2017) may be needed to make multi-specialty models viable.

5. Discussion

We presented two linked clinical solutions: (1) a single, calibrated medical VLM that runs an aware model-card–matching workflow, routing an input image to a model-card id—or abstaining and terminating when appropriate—and (2) the same VLM used as a specialty-specific downstream model with performance competitive with task-specific models.

For (Solution 1), the workflow is designed to streamline selection for data scientists by providing: *safety and trust* (stagewise decisions are visible throughout the pipeline), *robustness* (fewer incorrect selections via the combined use of stagewise prompts and the answer-selector logic), *scalability* (flexibility to add stages, descriptors, or model cards, or to swap in a more mature selector), and *speed* (a minimalist design with fewer moving parts than recent multi-agent pipelines (Shimgekar et al., 2025)).

For (Solution 2), specialty-specific models offer a practical first step toward automated deployment. We make this step concrete by shifting the effort from designing a new model to engineering a task-specific prompt that aligns the VLM's output with the downstream objective. In practice, this process can increase throughput for data scientists and clinicians without sacrificing performance.

Limitations and future work MedGemma is pretrained on a fixed set of modalities and tasks; accordingly, it may not generalize to imaging types or findings outside its training distribution. In short, its inference and selection decisions are tied to its training data: if a modality or pathology is unseen or underrepresented, the model may fail to recognize it and either choose an imperfect model or default to "Other/None." This risk can be mitigated by enlarging the pretraining corpus or by adopting continual-learning methods that add new domains while preserving prior knowledge (e.g., Li and Hoiem (2017)). Another limitation is that our current model card database supports up to two tasks per model (e.g., detection followed by classification); in reality, a case might benefit from multiple models (e.g., detection, classification and grading). Extending the pipeline to return a composite plan (multiple models in se-

quence) is an interesting direction. It is also worth noting that while our system outputs justifications for model selection, the interpretability of the VLM's internal reasoning remains limited (a common issue with large neural models). Techniques like chain-of-thought prompting or explicability constraints could be applied so the model provides brief, stagewise reasoning—further improving transparency (Wei et al., 2022). Another consideration is the choice of thresholds τ_1, τ_2, τ_3. We converged to approximate values that work well based on our prompting strategy at each stage, but in practice they may need adjustment for different clinical contexts. A high-sensitivity application (where missing a disease is very costly) might use a lower τ_2 to rarely terminate at "Normal" unless almost certain, whereas a high-specificity scenario might use a higher τ to avoid false alarms. Finally, our pipeline is across three stages because our repository lookup is primarily keyed on modality and one primary finding. As we incorporate more complex model cards (e.g., some models might handle combinations of findings or require patient metadata), the prompt design might need to extend to additional stages or a more free-form query. Fortunately, the modular nature of our approach means we can extend the prompting strategy as needed, and the answer selector concept can generalize to any number of stages by always examining the confidence of alternate responses. We outline two complementary directions for deployment: (1) automate fine-tuning end to end—so deployment proceeds with minimal data-scientist intervention—by automatically selecting the dataset linked to the model card chosen in solution 1 and automatically generating the prompts required for fine-tuning; and (2) reduce inference latency by applying pruning methods tailored to large language models (e.g., SparseGPT Frantar and Alistarh (2023)).

References

Andrea Acevedo, Anna Merino, Santiago Alférez, Ángel Molina, Laura Boldú, and José Rodellar. A dataset of microscopic peripheral blood cell images for development of automatic recognition systems. *Data in brief*, 30:105474, 2020.

Aidoc. Intelligent orchestration for radiology ai. https://www.aidoc.com/ai-orchestration/, 2024. Accessed 2025-08-10.

Mauro Annarumma, Steve Withey, Richard Bakewell, Emanuele Pesce, Via Goh, and Giovanni Montana. Automated triaging of adult chest radiographs with deep artificial neural networks. *The Lancet Digital Health*, 1(7):e307–e316, 2019. doi: 10.1016/S2589-7500(19)30117-0. URL https://www.ncbi.nlm.nih.gov/pmc/articles/PMC6438359/.

Jorge Bernal, Javier Sánchez, and Fernando Vilarino. Towards automatic polyp detection with a polyp appearance model. *Pattern Recognition*, 45 (9):3166–3182, 2012.

Bart-Jan Boverhof, W Ken Redekop, Daniel Bos, Martijn PA Starmans, Judy Birch, Andrea Rockall, and Jacob J Visser. Radiology ai deployment and assessment rubric (radar) to bring value-based ai into radiological practice. *Insights into Imaging*, 15(1):34, 2024.

Adrian P Brady, Bibb Allen, Jaron Chong, Elmar Kotter, Nina Kottler, John Mongan, Lauren Oakden-Rayner, Daniel Pinto Dos Santos, An Tang, Christoph Wald, et al. Developing, purchasing, implementing and monitoring ai tools in radiology: practical considerations. a multi-society statement from the acr, car, esr, ranzcr & rsna. *Canadian Association of Radiologists Journal*, 75 (2):226–244, 2024.

buoy health. buoy health solutions. https://www.buoyhealth.com, 2025. Accessed: 2025-08-12.

Rich Caruana. Multitask learning. *Machine Learning*, 28(1):41–75, 1997. doi: 10.1023/A:1007379606734.

Angel Cruz-Roa, Ajay Basavanhally, Fabio González, Hannah Gilmore, Michael Feldman, Shridar Ganesan, Natalie Shih, John Tomaszewski, and Anant Madabhushi. Automatic detection of invasive ductal carcinoma in whole slide images with convolutional neural networks. In *Medical imaging 2014: Digital pathology*, volume 9041, page 904103. SPIE, 2014.

DC Dataset. The 2nd diabetic retinopathy–grading and image quality estimation challenge, 2020.

Tim Dettmers, Artidoro Pagnoni, Ari Holtzman, and Luke Zettlemoyer. Qlora: Efficient finetuning of quantized llms, 2023. *URL https://arxiv.org/abs/2305.14314*, 2, 2023.

Elias Frantar and Dan Alistarh. Sparsegpt: Massive language models can be accurately pruned in one-shot. In *International conference on machine learning*, pages 10323–10337. PMLR, 2023.

Garner. Garner solutions. https://www.getgarner.com, 2025. Accessed: 2025-08-12.

Yonatan Geifman and Ran El-Yaniv. Selectivenet: A deep neural network with an integrated reject option. In *ICML*, pages 2151–2159, 2019.

Kristoffer Lindskov Hansen, Michael Bachmann Nielsen, and Caroline Ewertsen. Ultrasonography of renal lymphoma (image). Wikimedia Commons. Available at https://commons.wikimedia.org/wiki/File:Ultrasonography_of_renal_lymphoma.jpg, 2015. CC BY 4.0. Accessed: 2025-08-09. Source: "Ultrasonography of the Kidney: A Pictorial Review", Diagnostics 6(1):2, doi:10.3390/diagnostics6010002.

Fabian Isensee, Paul F. Jäger, Simon A. A. Kohl, Jens Petersen, and Klaus H. Maier-Hein. nnu-net: a self-configuring method for deep learning-based biomedical image segmentation. *Nature Methods*, 18:203–211, 2021. doi: 10.1038/s41592-020-01008-z.

Jakob Nikolas Kather, Johannes Krisam, Pornpimol Charoentong, Tom Luedde, Esther Herpel, Cleo-Aron Weis, Timo Gaiser, Alexander Marx, Nektarios A Valous, Dyke Ferber, et al. Predicting survival from colorectal cancer histology slides using deep learning: A retrospective multicenter study. *PLoS medicine*, 16(1):e1002730, 2019.

Daniel S Kermany, Michael Goldbaum, Wenjia Cai, Carolina CS Valentim, Huiying Liang, Sally L Baxter, Alex McKeown, Ge Yang, Xiaokang Wu, Fangbing Yan, et al. Identifying medical diagnoses and treatable diseases by image-based deep learning. *cell*, 172(5):1122–1131, 2018.

James Kirkpatrick, Razvan Pascanu, Neil Rabinowitz, Joel Veness, Guillaume Desjardins, Andrei A. Rusu, Kieran Milan, John Quan, Tiago Ramalho, Agnieszka Grabska-Barwinska, et al. Overcoming catastrophic forgetting in neural networks. *Proceedings of the National Academy of Sciences*, 114(13):3521–3526, 2017. doi: 10.1073/pnas.1611835114.

Kaidong Li, Mohammad I Fathan, Krushi Patel, Tianxiao Zhang, Cuncong Zhong, Ajay Bansal, Amit Rastogi, Jean S Wang, and Guanghui Wang. Colonoscopy polyp detection and classification: Dataset creation and comparative evaluations. *Plos one*, 16(8):e0255809, 2021.

Zhizhong Li and Derek Hoiem. Learning without forgetting. *IEEE transactions on pattern analysis and machine intelligence*, 40(12):2935–2947, 2017.

Vebjorn Ljosa, Katherine L Sokolnicki, and Anne E Carpenter. Annotated high-throughput microscopy image sets for validation. *Nature methods*, 9(7):637, 2012.

Mage AI. How long does it take to build an ml model? https://m.mage.ai/how-long-does-it-take-to-build-an-ml-model-d68b8afa50a5, 2025. Accessed: 2025-08-12.

Xueyan Mei, Philip M. Robson, Yang Yang, Zelong Liu, et al. Radimagenet: An open radiologic deep learning research dataset for effective transfer learning. *Radiology: Artificial Intelligence*, 4(5): e210315, 2022. doi: 10.1148/ryai.210315. URL https://pubmed.ncbi.nlm.nih.gov/36204533/.

Pablo Mesejo, Daniel Pizarro, Armand Abergel, Olivier Rouquette, Sylvain Beorchia, Laurent Poincloux, and Adrien Bartoli. Computer-aided classification of gastrointestinal lesions in regular colonoscopy. *IEEE transactions on medical imaging*, 35(9):2051–2063, 2016.

Margaret Mitchell, Simone Wu, Andrew Zaldivar, Parker Barnes, Lucy Vasserman, Ben Hutchinson, Elena Spitzer, Inioluwa Deborah Raji, and Timnit Gebru. Model cards for model reporting. In *Proceedings of the Conference on Fairness, Accountability, and Transparency (FAT* 2019)*, pages 220–229. ACM, 2019. doi: 10.1145/3287560.3287596.

Mukund Poddar, Jayson S. Marwaha, William Yuan, Santiago Romero-Brufau, and Gabriel A. Brat. An operational guide to translational clinical machine learning in academic medical centers. *npj Digital Medicine*, 7(1):129, 2024. doi: 10.1038/s41746-024-01094-9.

Project MONAI. Monai deploy app sdk. https://github.com/Project-MONAI/monai-deploy-app-sdk, 2023. Accessed 2025-08-10.

Sylvestre-Alvise Rebuffi, Alexander Kolesnikov, Georg Sperl, and Christoph H. Lampert. icarl: Incremental classifier and representation learning. In *Proceedings of the IEEE Conference on Computer Vision and Pattern Recognition (CVPR)*, pages 2001–2010, 2017. doi: 10.1109/CVPR.2017.200.

D. Sculley, G. Holt, D. Golovin, E. Davydov, T. Phillips, D. Ebner, V. Chaudhary, M. Young, J.-F. Crespo, and D. Dennison. Hidden technical debt in machine learning systems. In *NeurIPS*, 2015.

Andrew Sellergren, Sahar Kazemzadeh, Tiam Jaroensri, Atilla Kiraly, Madeleine Traverse, Timo Kohlberger, Shawn Xu, Fayaz Jamil, Cían Hughes, Charles Lau, et al. Medgemma technical report. *arXiv preprint arXiv:2507.05201*, 2025. URL https://arxiv.org/abs/2507.05201.

Yongliang Shen, Kaitao Song, Xu Tan, Dongsheng Li, Weiming Lu, and Yueting Zhuang. Hugginggpt: Solving ai tasks with chatgpt and its friends in hugging face. *Advances in Neural Information Processing Systems*, 36:38154–38180, 2023.

Soorya Ram Shimgekar, Shayan Vassef, Abhay Goyal, Navin Kumar, and Koustuv Saha. Agentic ai framework for end-to-end medical data inference. *arXiv preprint arXiv:2507.18115*, 2025. URL https://arxiv.org/abs/2507.18115.

Peng Wang, Shuai Bai, Sinan Tan, Shijie Wang, Zhihao Fan, Jinze Bai, Keqin Chen, Xuejing Liu, Jialin Wang, Wenbin Ge, et al. Qwen2-vl: Enhancing vision-language model's perception of the world at any resolution. *arXiv preprint arXiv:2409.12191*, 2024.

Xiaosong Wang, Yifan Peng, Le Lu, Zhiyong Lu, Mohammadhadi Bagheri, and Ronald M Summers. Chestx-ray8: Hospital-scale chest x-ray database and benchmarks on weakly-supervised classification and localization of common thorax diseases. In *Proceedings of the IEEE conference on computer vision and pattern recognition*, pages 2097–2106, 2017.

Jason Wei, Xuezhi Wang, Dale Schuurmans, Maarten Bosma, Ed H. Chi, Quoc V. Le, Denny Zhou, et al. Chain-of-thought prompting elicits reasoning in large language models. *arXiv preprint arXiv:2201.11903*, 2022. URL https://arxiv.org/abs/2201.11903.

Wikimedia Foundation. Wikimedia commons. https://commons.wikimedia.org/, 2025. Accessed: 2025-08-16.

Martin J. Willemink, Wojciech A. Koszek, Cailin Hardell, Jie Wu, Dominik Fleischmann, Hugh Harvey, Les R. Folio, Ronald M. Summers, Daniel L. Rubin, and Matthew P. Lungren. Preparing medical imaging data for machine learning. *Radiology*, 295(1):4–15, 2020. doi: 10.1148/radiol.2020192224.

Hanwen Xu, Naoto Usuyama, Jaspreet Bagga, Sheng Zhang, Rajesh Rao, Tristan Naumann, Cliff Wong, Zelalem Gero, Javier González, Yu Gu, et al. A whole-slide foundation model for digital pathology from real-world data. *Nature*, 630(8015):181–188, 2024.

Haiyang Yu, Siyang Yi, Ke Niu, Minghan Zhuo, and Bin Li. Umit: Unifying medical imaging tasks via vision–language models. *arXiv preprint arXiv:2503.15892*, 2025. URL https://arxiv.org/abs/2503.15892.

Yuhao Zhang, Hang Jiang, Yasuhide Miura, Christopher D. Manning, and Curtis P. Langlotz. Contrastive learning of medical visual representations from paired images and text. In *Proceedings of the Machine Learning for Healthcare Conference*, volume 182 of *Proceedings of Machine Learning Research*, pages 1–24, 2022. URL https://proceedings.mlr.press/v182/zhang22a/zhang22a.pdf.